Journal of Physics: Conference Series **635** (2015) 012011 doi:10.1088/1742-6596/635/1/012011

# Forward-angle electron spectroscopy in heavy-ion atom collisions studied at the ESR

**P-M Hillenbrand[1], S Hagmann[1], Yu A Litvinov[1], and Th Stöhlker[1,3,4]**

[1]GSI Helmholtzzentrum für Scherionenforschung, 64291 Darmstadt, Germany
[3]Helmholtz-Institut Jena, 07743 Jena, Germany
[4]Institut für Optik und Quantenelektronik, Friedrich-Schiller-Universität Jena, 07743 Jena, Germany

E-mail: p.m.hillenbrand@gsi.de

**Abstract.** The collision system $U^{88+} + N_2$ at a low-relativistic projectile energy of 90 MeV/u has been analyzed experimentally and theoretically with respect to fast electrons emitted with a velocity $v_e$ close to the projectile velocity, $v_p \approx v_e$, at an observation angle of $\vartheta_e \approx 0°$, i.e., in the direction of the projectile beam. Three distinct processes are identified, where each of the underlying charge-transfer mechanisms leads to a characteristic feature in the asymmetry of the observed electron energy distribution. The experimental results for each of the three processes are compared to the corresponding theoretical models.

## 1. Introduction

In collisions of heavy, highly-charged projectile ions with atomic targets, the energy distribution of the emitted electrons is a characteristic observable and highly sensitive to distinguish the underlying elementary processes. The system of beryllium-like $U^{88+}$-projectiles colliding at an energy of 90 MeV/u with a target of $N_2$ provides a unique possibility of observing three distinct charge-transfer processes with emission of a cusp electron, i.e., an electron with a velocity $v_e$ similar to the projectile velocity, $v_p \approx v_e$, emitted parallel to the projectile beam at a polar angle of $\vartheta_e \approx 0°$:

(a) The process of **electron loss to continuum** (ELC) corresponds to the ionization of the projectile ion, where an electron with binding energy $E_p^b$ is transfered into the projectile continuum during the collision with the target,

$$U^{88+} + N_2 \rightarrow U^{89+} + [N_2]^* + e^-.$$

It is dominated by a comparably small momentum transfer proportional to $\frac{E_p^b}{v_p}$. The unambiguous identification of ELC requires a coincidence measurement of the emitted electron and the up-charged projectile [1, 2]. Previous studies include few-electron light projectiles [3] and many-electron heavy projectiles [4], but few-electron heavy projectiles were not experimentally studied up to now. Experimental data for the characteristics of the emitted electron provide stringent tests for theory well beyond total ionization cross sections. Moreover, for a reliable theoretical model the description of the ionization of heavy projectiles requires a fully relativistic treatment of the collision process, which is only available for few-electron projectiles up to now [5].

(b) The process of **electron capture to continuum** (ECC) corresponds to the capture of a target electron into the projectile continuum:

$$U^{88+} + N_2 \rightarrow U^{88+} + \left[N_2^+\right]^* + e^-.$$

It requires a large momentum transfer proportional to $v_p$ onto the target atom in order to facilitate momentum balance during the electron transfer to the projectile continuum. Since ECC is the dominating process at low collision velocities, it is well know since several decades [6]. Also for ECC, previous studies used light ions [1, 7] or dressed heavy ions [8], while experimental data for highly-charged heavy projectiles were not available up to now.

(c) The process of **radiative electron capture to continuum** (RECC) corresponds to the capture of a target electron into the projectile continuum, while the excess energy is carried away by a photon:

$$U^{88+} + N_2 \rightarrow U^{88+} + \left[N_2^+\right]^* + e^- + \gamma.$$

Due to the additional degree of freedom in the energy of the emitted photon, no momentum transfer is required. As for the homologue process of radiative capture of a target electron into a bound state of the projectile, REC [9], RECC dominates over its non-radiative counterpart towards relativistic collision energies. It was shown, that RECC can be described as the high-energy end-point of electron-nucleus bremsstrahlung in inverse kinematics [10]. Experimental data for RECC comprise coincidence measurements of the electron energy distribution at $\vartheta_e = 0°$ as well as the photon energy and angular distribution, and provide stringent tests for the relativistic theory of the fundamental process of electron-nucleus bremsstrahlung, complementary to bremsstrahlung experiments in classical geometry.

At the experimental storage ring (ESR) of the heavy-ion accelerator facility GSI Helmholtzzentrum für Schwerionenforschung, a dedicated magnetic electron spectrometer was built downstream from the gas-jet target, which enabled the measurement of high-energy

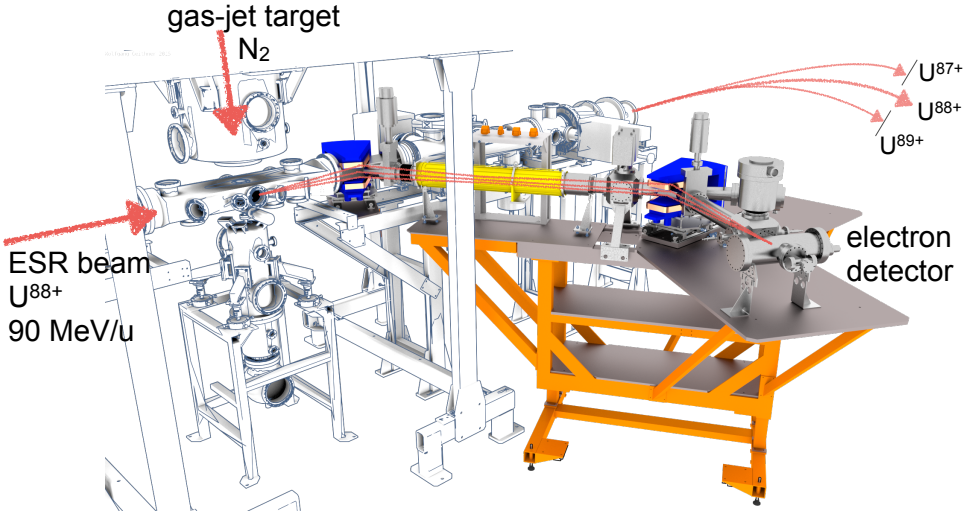


Figure 1: Magnetic forward-angle electron spectrometer at the experimental storage ring (ESR): The interaction point was defined by the overlap between the ion-beam from the ESR and the supersonic gas-jet target. Electrons emitted from the interaction point into the forward direction were separated from the ion beam by the first dipole magnet (blue) and were then guided by a magnetic quadrupole triplet (yellow) and a second dipole magnet (blue) onto the position sensitive electron detector. Up- and down-charged projectiles, $U^{89+}$ and $U^{87+}$, were separated from $U^{88+}$ ions by the subsequent dipole magnet of the ESR. Not shown are the x-ray detectors mounted in the horizontal plane around the interaction point.

electrons emitted in ion-atom collisions within a small cone around the forward direction. The three listed processes were studied using this electron spectrometer in combination with detectors for emitted x rays and charge-exchanged projectiles. Within the study presented here, it was shown that each of the three processes is characterized by a unique electron-cusp shape, being a clear messenger for the underlying charge-exchange mechanism.

## 2. Experiment

Traditionally, spectroscopy of electrons emitted from the *projectile* during non-relativistic ion-atom collisions at energies not exceeding a few MeV/u is performed by electrostatic spectrometers, with typical electron energies of hundreds of eV [1–4, 6–8]. For comparison, electrons emitted from the *target* with energies of a few eV are typically observed by reaction microscopes [12]. However, towards relativistic projectile energies, the energy of electrons emitted from the *projectile* is so high that it can only be analyzed by a magnetic spectrometer. The highest yield of electrons as well as a reduced kinematical energy broadening is given at an observation angle of $\vartheta_e = 0°$ with respect to the projectile beam [13].

For the experiment presented here, a magnetic forward-angle electron spectrometer was installed at the ESR. In the ESR, an electron cooled beam of $U^{88+}$ was intersected with a supersonic gas-jet target of $N_2$. Electrons emitted from the interaction point within a polar angle of $\vartheta_e = 0° - 2.4°$ and an azimuthal angle of $\varphi_e = 0° - 360°$ were guided by a sequence of a 60°-dipole magnet, a magnetic iron-free quadrupole triplet, and a second 60°-dipole magnet onto a position sensitive electron detector, as shown in figure 1. The energy distribution of the emitted electrons was measured by counting the detected electrons as a function of the magnetic fields applied to the spectrometer, while each step was characterized by a momentum

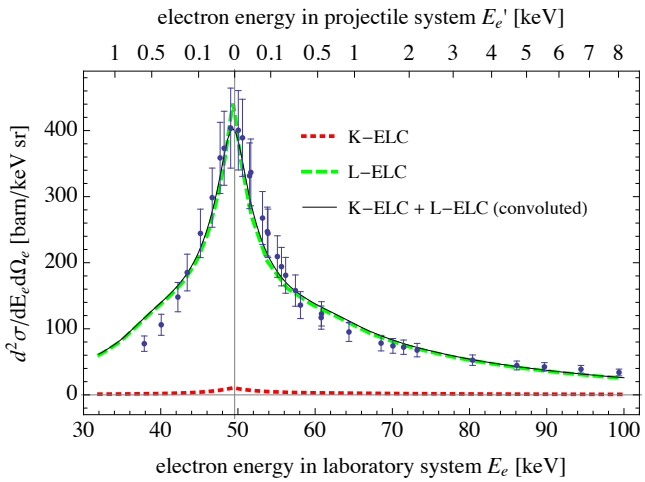


(a) Double-differential cross section $d^2\sigma/dE_e d\Omega_e$ in the *laboratory frame* as a function of the kinetic energy of the emitted electron $E_e$ observed at an angle of $\vartheta_e = 0° - 2.4°$. Displayed are the experimental data (blue symbols), the theory for $K$-ELC (red dotted line), the theory for $L$-ELC (green dashed line), and the sum of the contributions of $K$- and $L$-ELC convoluted with the energy resolution of the spectrometer (black solid line). The experimental relative cross sections were normalized to the theory calculated using fully relativistic Dirac wave-functions.

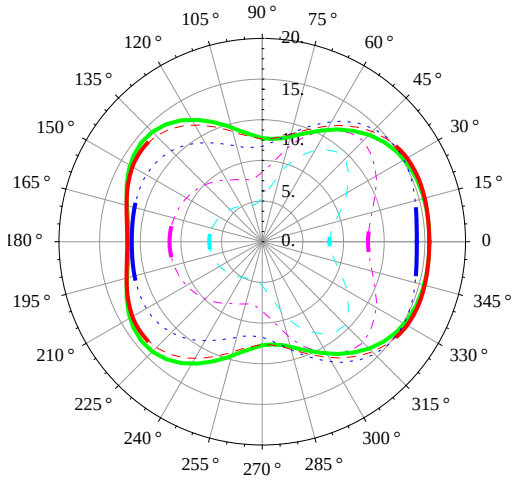


(b) Double-differential cross section $d^2\sigma/dE'_e d\Omega'_e$ in the *projectile frame* for $L$-ELC as a function of $\vartheta'_e$ for different electron emission energies: $E'_e = 0.047$ keV (solid green line), $E'_e = 0.192$ keV (short-dashed red line), $E'_e = 1.094$ keV (dotted blue line), $E'_e = 5.054$ keV (dot-dashed magenta line), $E'_e = 11.542$ keV (long-dashed cyan line). The intervals of the angular distributions marked in bold fall into the angular acceptance of the electron spectrometer in the laboratory system.

Figure 2: Electron loss to continuum: $U^{88+} + N_2 \rightarrow U^{89+} + [N_2]^* + e^-$, results from ref. [11].

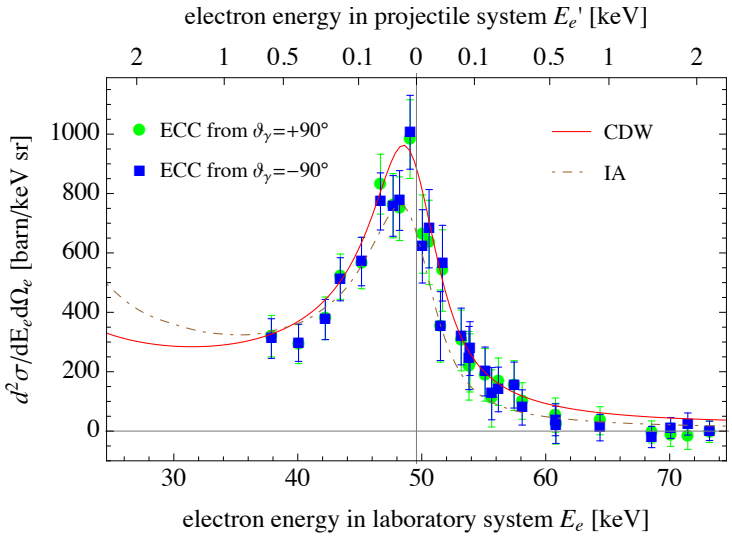


Figure 3: Electron-capture to continuum: $U^{88+} + N_2 \rightarrow U^{88+} + \left[N_2^+\right]^* + e^-$, results from ref. [15]. Shown is the double-differential cross section $d^2\sigma/dE_e d\Omega_e$ as a function of the kinetic energy $E_e$ of the emitted electron observed under $\vartheta_e = 0° - 2.4°$. The experimental data for ECC was deduced by subtracting from the non-coincident electron spectrum the coincident events from ELC and the extrapolated coincident events from RECC observed at $\vartheta_\gamma = +90°$ (green circles) and $\vartheta_\gamma = -90°$ (blue squares). The results of the continuum-distorted-wave theory (red solid line) and the impulse approximation theory (brown dashed line) are given. The experimental relative cross sections were normalized to the average of both theories.

acceptance of $\Delta p_e/p_e = 0.02$. Along with the emitted electrons, the up- and down-charged projectiles, $U^{89+}$ and $U^{87+}$, were observed as well as x rays emitted from the interaction point, such that coincident events between the different detectors could be identified. Details of the experimental setup are given in refs. [11, 14, 15].

## 3. Results

### *3.1. Electron loss to continuum*

In figure 2(a) the experimental results for the process of ELC are shown, in comparison with the theoretical prediction for the contribution of $K$-ELC and $L$-ELC. As can be seen from the theoretical electron distribution in the (primed) projectile frame for $L$-ELC shown in figure 2(b), the low-energy fraction of the ionized electrons is emitted almost isotropically, with a clear signature of the node in the $2s$ wave-function of the $U^{88+}(1s^2 2s^2)$ ion. Consequently, the electron cusp in the laboratory frame is quasi-symmetric.

The theoretical calculations were performed in the projectile frame for a bare $N^{7+}$-nucleus impinging on a $U^{88+}$ ion. In contrast to the other two processes, the effect of the target electrons is negligible here. The interaction between the electrons of the projectile and the nucleus of the target was described within first order perturbation theory by applying one-electron Dirac wave-functions [5]. A good agreement between the experimental data and the fully relativistic calculation was achieved. Details of this study are given in ref. [11].

### *3.2. Electron capture to continuum*

In figure 3 the experimental results for the process of ECC are shown, in comparison with two theoretical models. The electron energy distribution exhibits a characteristic asymmetry with a preference towards the low-energy slope. In the projectile frame, the target electrons perform Coulomb scattering in the field of the projectile, preferably under small scattering angles, which after transformation into the laboratory frame leads to the observed cusp asymmetry.

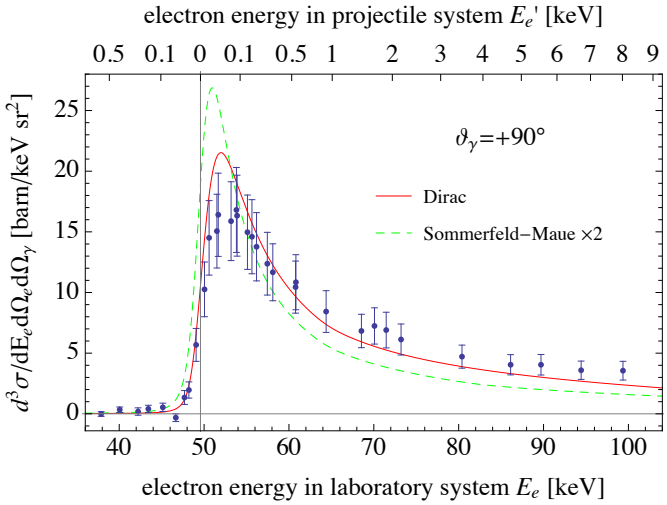


(a) Triple-differential cross sections $d^3\sigma/dE_e d\Omega_e d\Omega_\gamma$ in the *laboratory frame* as a function of the kinetic energy of the emitted electron $E_e$ observed under $\vartheta_e = 0^\circ - 2.4^\circ$ for photons emitted at $\vartheta_\gamma = 90^\circ$. Displayed are the experimental cross sections (blue symbols), and the theoretical calculations done by applying fully relativistic Dirac wave-functions (red solid line) and by applying semi-relativistic Sommerfeld-Maue wave-functions multiplied by 2 (green dashed line). The experimental relative cross sections were normalized to Dirac theory.

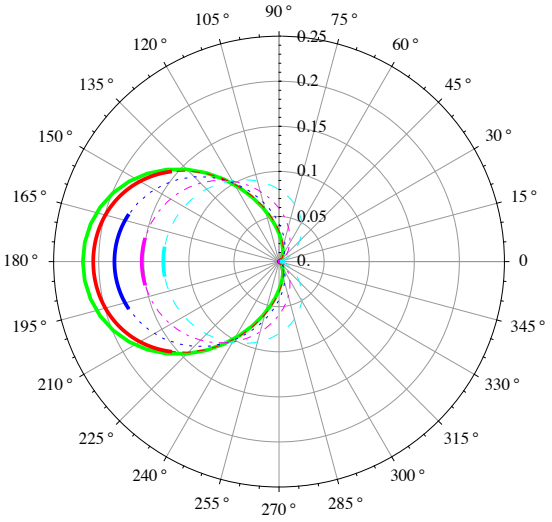


(b) Triple-differential cross sections $d^3\sigma/dE'_e d\Omega'_e d\Omega'_\gamma$ in the *projectile frame* as a function of $\vartheta'_e$ for $\vartheta'_\gamma = 65.7^\circ$ and $\varphi_\gamma = 0^\circ$, and for different kinetic energies of the emitted electron: $E'_e = 0.06$ keV (green solid line), $E'_e = 0.2$ keV (red short-dashed line), $E'_e = 1.0$ keV (blue dotted line), $E'_e = 4.0$ keV (magenta dot-dashed line), and $E'_e = 10.0$ keV (cyan long-dashed line). The electron distributions are averaged over $\varphi'_e = 0^\circ - 360^\circ$. The intervals of the angular distributions marked in bold fall into the angular acceptance of the electron spectrometer in the laboratory system.

Figure 4: Radiative electron capture to continuum: $U^{88+} + N_2 \rightarrow U^{88+} + \left[N_2^+\right]^* + e^- + \gamma$, results from ref. [14].

In the applied theoretical models, the continuum-distorted-wave model (CDW) comprised non-relativistic wave-functions [16], but relativistic kinematics. In the impulse approximation (IA), semi-relativistic Sommerfeld-Maue wave-functions were used [17]. Since the electron energy spectrum predominately depends on the initial momentum distribution of the bound electrons in the nitrogen target atom, which can well be described by non-relativistic wave-functions, both theories are in reasonably good agreement with experiment. For ECC, an improved theory would require a fully relativistic two-center approach. Details of this study are given in ref. [15].

### *3.3. Radiative electron capture to continuum*

In figure 4(a) the experimental results in the laboratory frame for the process of RECC are shown in comparison with two theoretical models. The electron distribution shown in figure 4(b) illustrates that in the projectile frame the electrons are emitted into the backward direction, i.e., $\vartheta'_e \approx 180^\circ$. These large scattering angles are an indication for the small impact parameters involved, since the coupling of the electron to the electromagnetic field of the emitted photon occurs dominantly in the strongest part of the Coulomb field of the $U^{88+}$ ion. The transformation of the theoretical triple-differential cross section from the projectile frame, i.e., the electron scattering frame, to the laboratory frame involves a rotation by of the polar angle $\vartheta'_e$ by 180°, such that the distribution of backward emitted electrons in the projectile frame lead to a strong asymmetry of the electron energy distribution in the laboratory frame with a dominance of electrons towards the high-energy slope of the cusp.

The theoretical triple-differential cross sections in the projectile frame given in figure 4(b) are

based on a fully relativistic calculation using Dirac wave-functions for the continuum states of the $U^{88+}$ ion [18]. For RECC, the nitrogen target merely serves as a source of (quasi-)free electrons. For this calculation, bremsstrahlung theory was used for an incoming electron with a kinetic energy of 50 keV scattering off a $U^{88+}$ ion, such that a fraction of the kinetic energy is transfered onto the emitted bremsstrahlung photon. The limiting case, where (almost) all kinetic energy is transfered from the incoming electron to the emitted photon, is the high-energy endpoint of electron-nucleus bremsstrahlung. When the outgoing electron has (almost) no kinetic energy, it populates a low-energy continuum state of the projectile. This case can only be studied in inverse kinematics using highly-charged ions, as was realized in our experiment. The calculations based on fully relativistic Dirac theory are in good agreement with the experimental data. Furthermore, the measured spectra were compared to calculations applying semi-relativistic Sommerfeld-Maue wave-functions [19]. The results show that the validity of these calculations, which were used in the previous study of ref. [10], is not confirmed by the experimental data. Details of this investigation of RECC including the photon angular distribution are given in ref. [14].

## 4. Summary and Outlook

Within this study, three processes involving the emission of a cusp electron were analyzed for $U^{88+}$-projectiles colliding with a supersonic gas-jet target of $N_2$. The characteristic features of the cusp shape were traced back to the underlying charge-transfer mechanisms. The corresponding theoretical electron distributions in the projectile frame provided an additional understanding of the collision processes. An increased complexity is given when *multi-electron* heavy projectiles are studied. Experimental data of the electron emission spectra in collisions of $U^{28+}$ with atomic targets are currently being analyzed [20]. Ideas of transferring the concept of a magnetic electron spectrometer at a heavy-ion storage ring towards a magnetic positron spectrometer at a high-energy heavy-ion storage ring are also being discussed [21].

## Acknowledgments

This work was supported by the Helmholtz-CAS Joint Research Group HCJRG-108. The authors thank W. Geithner for his assistance with figure 1.

## References

[1] Breinig M *et al.* 1982 *Phys. Rev. A* **25** 3015–3048
[2] Liao C *et al.* 1995 *Nucl. Instrum. Methods B* **98** 324–327
[3] Vane C R *et al.* 1978 *Phys. Rev. Lett.* **40** 1020–1023
[4] Andersen L H *et al.* 1984 *Phys. Rev. Lett.* **52** 518–521, Schneider D *et al.* D 1993 *Phys. Rev. A* **47** 3945–3950
[5] Voitkiv A B 2004 *Phys. Rep.* **392** 191–277
[6] Rudd M E, Sautter C A and Bailey C L 1966 *Phys. Rev.* **151** 20–27
[7] Stolterfoth N 1995 *Phys. Rev. A* **52** 3796–3802
[8] Schneider D *et al.* 1989 *Phys. Rev. A* **40** 2971–2975
[9] Eichler J and Stöhlker T 2007 *Phys. Rep.* **439** 1–99
[10] Nofal M *et al.* 2007 *Phys. Rev. Lett.* **99** 163201
[11] Hillenbrand P M *et al.* 2014 *Phys. Rev. A* **90** 042713
[12] Ullrich J *et al.* 2003 *Rep. Prog. Phys.* **66** 1463-1545
[13] Stolterfoth N 1987 *Phys. Rep.* **146** 315–424, Zouros T J M *et al.* 2008 *Phys. Rev. A* **77** 050701
[14] Hillenbrand P M *et al.* 2014 *Phys. Rev. A* **90** 022707
[15] Hillenbrand P M *et al.* 2015 *Phys. Rev. A* **91** 022705
[16] Monti J M, Rivarola R D and Fainstein P D 2011 *J. Phys. B* **44** 195206
[17] Jakubassa-Amundsen D H 2007 *Eur. Phys. J. D* **41** 267–274
[18] Müller R A, Yerokhin, V A and Surzhykov A 2014 *Phys. Rev. A* **90** 032707
[19] Jakubassa-Amundsen D H 2003 *J. Phys. B* **36** 1971–1989
[20] Hillenbrand P M *et al. in preparation*
[21] Hillenbrand P M *et al.* 2015 *Phys. Scr. in press*